

Morphological characterization of very small embryonic-like stem cells (VSELs) by ImageStream system analysis

Ewa K. Zuba-Surma^{a,*}, Magdalena Kucia^a, Ahmed Abdel-Latif^b, Buddhadeb Dawn^b,
Brian Hall^c, Rajesh Singh^d, James W. Lillard, Jr^d, Mariusz Z. Ratajczak^{a,*}

^a Stem Cell Biology Institute, University of Louisville, Louisville, KY, USA

^b Institute of Molecular Cardiology, University of Louisville, Louisville, KY, USA

^c Amnis Corporation, Seattle, WA 98121, USA

^d Brown Cancer Center, University of Louisville, Louisville, KY, USA

Received: June 25, 2007; Accepted: October 30, 2007

Abstract

Recently, our group purified a rare population of primitive Sca1⁺/Lin⁻/CD45⁻ cells from murine bone marrow by employing multi-parameter cell sorting. Based on flow cytometric and gene expression analysis, these cells have been shown to express several markers of embryonic stem cells and were accordingly termed Very Small Embryonic-Like stem cells (VSELs). In order to better characterize VSELs, we focused on their morphological parameters (*e.g.* diameter, nuclear to cytoplasmic ratio, cytoplasmic area) as well as expression of Oct-4. To examine the morphological features of VSELs, we employed a multi-dimensional approach, including (*i*) traditional flow cytometry, (*ii*) a novel approach, which is ImageStream (IS) cytometry and (*iii*) confocal microscopy. We demonstrate by all of the sensitive and precise methods employed, that VSELs are a population of very small cells, which are significantly smaller than haematopoietic stem cells (HSC) (3.63 ± 0.09 versus 6.54 ± 0.17 μm in diameter). They also exhibit higher nuclear to cytoplasmic ratio and lower cytoplasmic area as compared with HSCs and mature granulocytes. Besides confirming the size characteristics, confocal microscopic analysis also confirmed that VSELs express Oct-4, a marker of pluripotent embryonic stem cells. Morphological examination reveals that VSELs are unusually small eukaryotic cells that possess several characteristics of embryonic cells. Thus, FACS-based sorting strategies should consider that adult tissues harbour small primitive cells that are larger than platelets and smaller than erythrocytes.

Keywords: CXCR4 • ImageStream • VSEL • Oct-4 • nuclear to cytoplasmic ratio • pluripotent cells

Introduction

Recently, our group purified a rare population of primitive non-haematopoietic Sca-1⁺/Lin⁻/CD45⁻

cells from murine bone marrow (BM) by multi-parameter fluorescence activated cell sorting (FACS) [1]. Based on transmission electron microscopic analysis showing primitive organization of chromatin, these cells were named very small embryonic-like stem cells (VSELs) [1–3]. Using real-time RT-PCR and immunohistochemistry we have also demonstrated that BM-derived VSELs highly express a multitude of pluripotent stem cell markers including SSEA-1, Oct-4, Nanog and Rex-1 [1]. Moreover, VSELs are also

*Correspondence to: Mariusz Z. RATAJCZAK M.D., Ph.D.,
or Ewa K. ZUBA-SURMA, Ph.D.,
Stem Cell Institute, James Graham Brown Cancer Center,
University of Louisville, 500 Floyd St., Louisville, KY
40202, USA.

Tel.: +50 2-85 2-34 86

Fax: +50 2-85 2-30 32

E-mail: mzrata01@louisville.edu or

ekzuba01@louisville.edu

doi: 10.1111/j.1582-4934.2007.00154.x

© 2008 The Authors

Journal compilation © 2008 Foundation for Cellular and Molecular Medicine/Blackwell Publishing Ltd

enriched for mRNA of genes associated with development of skeletal muscles (Myf-5, MyoD, Myogenin), heart (Nkx2.5/Csx, GATA-4, MEF-2C), neural cells (Nestin, GFAP), liver (CK19, α -fetoprotein), intestinal epithelium (Nkx 2-3, Tcf4, CDX1, Msi1h), skin epidermis (Trp63, Krt 2-6a, Krt 2-5, BNC) and endocrine pancreas (Nkx6.1, Pdx1, Ptf1) [1]. Furthermore, VSELs demonstrated several embryonic stem cell-like characteristics, including the capacity to form *in vitro* spheres resembling embryoid bodies which highly express the placental form of alkaline phosphatase and several genes involved in early gastrulation [4, 5]. We also confirmed their extensive pluripotency by demonstrating the ability of VSELs to differentiate into all three germ-layer lineages [1].

Unfortunately the FACS-based sorting strategy to isolate VSELs includes gating on region that contains mostly cell debris and only rare cellular events (2–6 μ m). Thus to optimize purity of VSELs sorting and to better characterize the morphological features of these cells, we employed a multi-dimensional approach (traditional flow cytometry, ImageStream cytometry analysis and confocal microscopy). Firstly, using classical flow cytometry we compared the exact size of phenotypically identified VSELs with standard beads with pre-defined sizes. Second, the novel technological approach, which is ImageStream (IS) allowed us to analyse these cells in flow in suspension [6–8]. IS technology combines the statistical power of large sample size analysis common to flow cytometry with the morphological features obtained by microscopic methods [6–8]. We employed IS to differentiate VSELs from cell debris as well as for estimating the true percentage of these cells. Using this technology, we also computed the nuclear to cytoplasmic (N/C) ratio, which has been proposed as an indicator of stemness of primitive cells and calculated cytoplasmic area. Finally, by employing confocal microscopy, we examined both the size as well as Oct-4 expression in VSELs.

All of these modalities employed simultaneously allowed us to achieve optimal gating, purification, and morphological characterization of VSELs at single cell level and confirmed their primitive/embryonic-like nature.

Material and methods

Animals

These experiments have been performed in accordance with the guidelines of the Laboratory Institutional Animal

Care and Use Committee (IACUC). The investigation conforms to the Guide for the Care and Use of Laboratory Animals published by the US National Institutes of Health (NIH Publication No. 85-23, revised 1996).

Isolation of BM cells, flow cytometric sorting and analysis

VSELs were isolated from BM of adult C57BL/6 mice (4–8 weeks old) (Jackson Laboratory, Bar Harbor, ME, USA). BM was flushed from tibias and femurs and full population of bone marrow mononuclear cells (BMMNCs) was obtained after lysis of RBCs using 1x BD Pharm Lyse Buffer (BD Pharmingen, San Jose, CA, USA). Cells were stained for CD45, Lineages markers, and Sca-1 for 30 min in medium containing 2% of fetal bovine serum (FBS). The following directly conjugated antimouse antibodies (mAbs) (BD Pharmingen, San Jose, CA, USA) were used to stain cells prior to FACS: rat anti-CD45 (APC-Cy7; clone 30-F11), anti-CD45R/B220 (PE; clone RA3-6B2), anti-Gr-1 (PE; clone RB6-8C5), anti-TCR $\alpha\beta$ (PE; clone H57-597), anti-TCR $\gamma\delta$ (PE; clone GL3), anti-CD11b (PE; clone M1/70), anti-Ter119 (PE; clone TER-119) and anti-Ly-6A/E (Sca-1) (biotin; clone E13-161.7, with streptavidin conjugated with PE-Cy5). Cells were then washed and re-suspended in RPMI 1640 medium with 10% of FBS and sorted by MoFlo cell sorter (Dako, Carpinteria, CA, USA). The Sca-1⁺/Lin⁻/CD45⁻ (VSELs) and Sca-1⁺/Lin⁻/CD45⁺ (HSCs, control) were isolated accordingly to the gating and sorting strategy summarized in Figure 1. We also used 7-aminoactinomycin D (7-AAD; Invitrogen; Molecular Probes; 40 μ M) to exclude dead cells from sorting (Fig. 1).

Confocal microscopic analysis

Freshly sorted Sca-1⁺/Lin⁻/CD45⁻ (VSELs) and Sca-1⁺/Lin⁻/CD45⁺ (HSCs, control) were plated for 24 hr on 22-mm-diameter plates coated with poly-L-lysine, fixed with 4% paraformaldehyde solution for 20 min and washed three times with phosphate-buffered saline (PBS). Following fixation, cells were permeabilized with 0.1% Triton X-100 (Sigma Aldrich, St. Louis, Missouri, USA) for 5 min. Before staining with specific antibodies, samples were blocked with 10% donkey serum (Jackson ImmunoResearch laboratories, West Grove, PA) for 30 min at room temperature to avoid non-specific binding. Then cells were incubated with primary antibodies against Oct-4 (1:200, mouse monoclonal IgG; Chemicon Int., Temecula, CA, USA) and CD45 (1:100, rat monoclonal IgG1, clone 30-F11, FITC-conjugated) (BD Pharmingen, San Jose, CA, USA) for 2 hrs at 37°C. Cells were washed with PBS followed by the addition of TRITC-conjugated secondary antibody (donkey anti-mouse IgG, Jackson ImmunoResearch, West Grove, PA) at

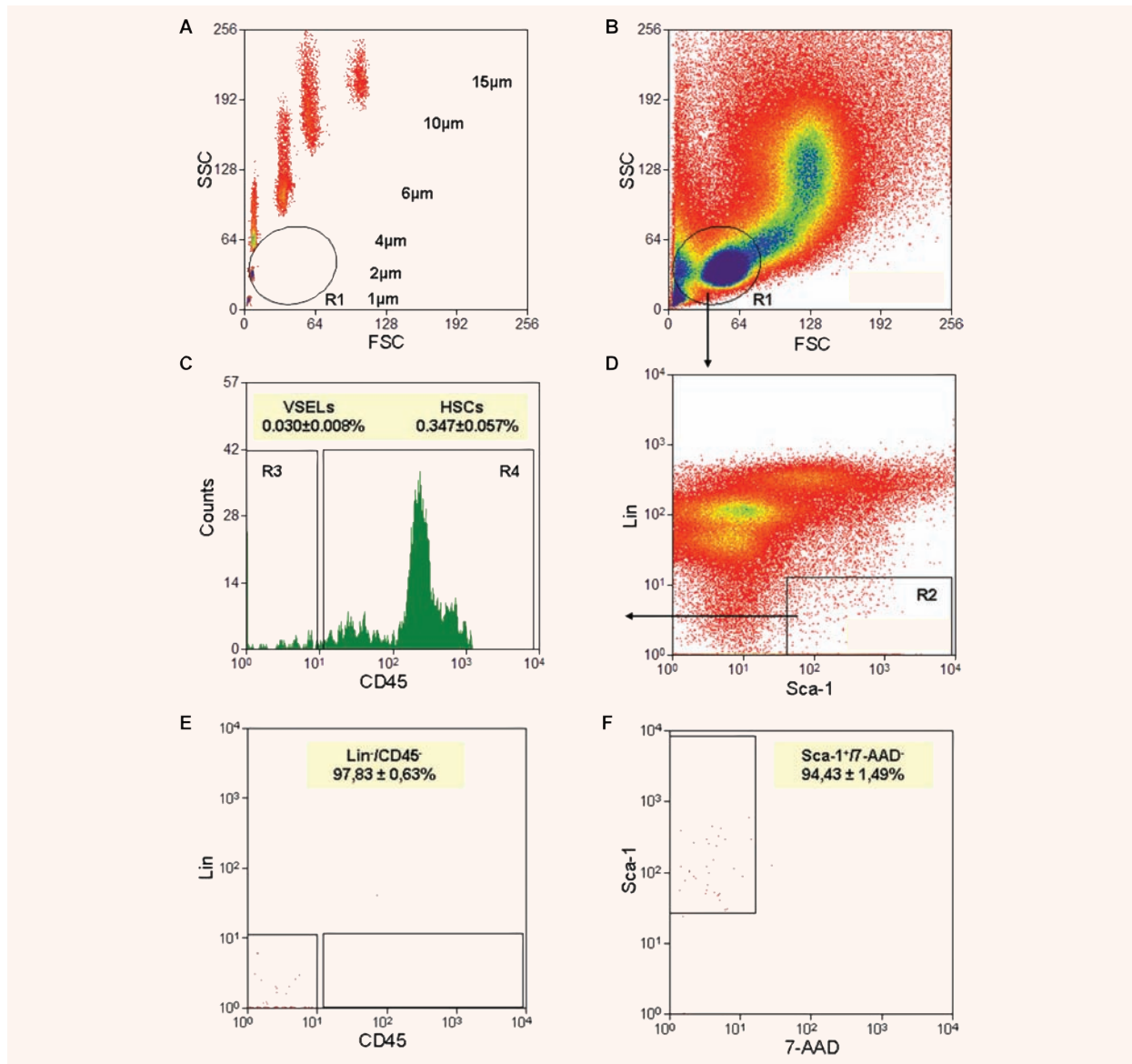


Fig. 1 Gating strategy for sorting VSELs by FACS. Bone marrow (BM)-derived VSELs were isolated from immunofluorescence stained full BMMNC population by FACS. Agranular, small events ranging from 2–10 μm were included into gate R1 after comparison with six differently sized beads particles with standard diameters of 1, 2, 4, 6, 10 and 15 μm (Flow Cytometry Size beads, Invitrogen; Molecular Probes, Carlsbad, Ca, USA) (**A**). Bone marrow mononuclear cells (BMMNC) were visualized by dot plots showing FSC (forward scatter) *versus* SSC (side scatter) signals, which are related to the size and granularity/complexity of the cell, respectively (**B**). Cells from region R1 were further analysed for Sca-1 and Lin expression and only Sca-1⁺/Lin⁻ events were included into region R2 (**D**). Population from region R2 was subsequently sorted based on CD45 marker expression into CD45⁻ and CD45⁺ subpopulations visualized on histogram (**C**; regions R3 and R4, respectively). Sca-1⁺/Lin⁻/CD45⁻ cells (VSELs) were sorted as events enclosed in logical gate including regions R1, R2 and R3, while Sca-1⁺/Lin⁻/CD45⁺ cells (HSCs) from gate including regions R1, R2 and R4. Percentages show the average content of each cellular subpopulation (\pm S.E.M.) in total BMMNC. Sorted VSELs were re-analysed to establish sorting purity according Lin, CD45 and Sca-1 markers as well as their viability by staining with 7-AAD (**E**, **F**). Percentages on these two panels present purity of VSELs in each marker and content of viable cells (Mean \pm S.E.M.). Cells were not fixed before staining with 7-AAD.

a concentration of 1:200 for 2 hrs at 37°C to visualize the staining with anti-Oct-4 antibody. Nuclei were stained with DAPI (Molecular Probes, Carlsbad, California, USA) for 10 min at 37°C. All immunofluorescence photomicrographs were acquired using a Zeiss LSM 510 confocal microscope (Carl Zeiss, Thornwood, New York, USA).

ImageStream system analysis

BM of adult C57BL/6 mice (4 weeks old, Jackson Laboratory, Bar Harbor, ME, USA) was isolated as described above for flow cytometric sorting and analysis. The full population of BMMNCs was obtained after lysis of red blood cell (RBCs) using 1x BD Pharm Lyse Buffer (BD Pharmingen). Blood was obtained from the inferior vena cava and left ventricular cavity of C57BL/6 mice (4–8 weeks old). Peripheral blood (PB) cells were obtained after lysis of RBCs using the above method. Among the different differentiated cell populations in blood, we elected to use granulocytes as controls for comparing cell size, N/C ratio, and cytoplasmic area. Nalm-6 cells, human B-ALL cell line, were used as an additional control. Total BM- and PB-derived cells were stained for CD45, lineage markers, and Sca-1 for analysis by ImageStream system. Based on the detection channels available for the IS system, the following directly conjugated monoclonal mAbs (BD Pharmingen, San Jose, CA, USA) were used for staining: rat anti-CD45 (FITC; clone 30-F11), anti-CD45R/B220 (PE; clone RA3-6B2), anti-Gr-1 (PE; clone RB6-8C5), anti-TCR $\alpha\beta$ (PE; clone H57-597), anti-TCR $\gamma\delta$ (PE; clone GL3), anti-CD11b (PE; clone M1/70), and anti-Ter119 (PE; clone TER-119). Staining for anti-Ly-6A/E (Sca-1) (biotin; clone E13-161.7) was followed by staining with streptavidin conjugated with PE-Cy5. Nalm-6 cells were stained against human CD19 (FITC; clone HIB19) and CD45 (PE; clone HI30; both antibodies purchased from BD Biosciences, San Jose, CA, USA). Cells were washed after staining, fixed with 4% paraformaldehyde for 20 min and then permeabilized with 0.1% Triton X-100 solution for 10 min. Stained cells were re-suspended in PBS for further analysis. 7-aminoactinomycin D (7-AAD; Invitrogen; Molecular Probes; 40 μ M) was added 5 min before analysis. Samples were run directly on ImageStream System 100 (Amnis Corporation, Seattle, WA, USA) without any cell classifier (instrument threshold).

Signals from FITC, PE, 7-AAD, and PE-Cy5 were detected by channels 3, 4, 5 and 6, respectively, while side scatter and brightfield images were collected in channels 1 and 2, respectively. The methodology was applied for experiments comparing the size, N/C ratio and cytoplasmic area of VSELs (Sca-1⁺/Lin⁻/CD45⁻) and HSCs (Sca-1⁺/Lin⁻/CD45⁺) with other cells (Figs. 5 and 7).

During BM-derived VSEL analysis, shown in Figures 4 and 6, the parameters of acquisition were attuned to detect and analyse very small events containing nuclei, which were negative for Linage markers and CD45 (*i.e.* Lin⁻/CD45⁻ cells). For this purpose the settings and threshold of the instrument were adjusted to exclude most of the Lin⁺/CD45⁺ events by decreasing the peak upper limit for channels detecting fluorescence signals from CD45 and Lin (FITC- channel 3 and PE- channel 4, respectively). Simultaneously, IS was configured to detect even very small events containing DNA, defined in the protocol as small areas of brightfield containing a nucleus. Because of these settings, not all BM-derived cells were detected by IS and the majority CD45⁺ and Lin⁺ events were not analysed. VSELs were detected among the Sca-1⁺/Lin⁻/CD45⁻ objects (Figs. 4 and 6).

On the brightfield single images, masks encompassing the entire cellular areas (eroded 5 pixels) were created by the ImageStream system software (IDEAS) software and were used to calculate the area of cells. Similarly, the nuclear area was calculated by automatic masks created on the 7-AAD nuclear images (morphology mask). Cytoplasmic area was computed by subtracting the nuclear area from the total area of the cell. The N/C ratio was computed as the ratio between nuclear and cytoplasmic areas.

Statistical analysis

Data are expressed as mean \pm S.E.M. A *P*-value <0.05 was considered statistically significant. All statistical analyses were performed using the Origin (version 5.0) statistical software (Northampton, MA, USA).

Results

VSELs are much smaller than HSCs

We employed a novel size-based approach controlled by size bead markers for isolating rare and small VSELs from murine BM by FACS (Fig. 1A). The overall sorting strategy is based on gating in regions containing small events (2–10 μ m) - as indicated on the dot plot (region R1) (Fig. 1B). This region contains mostly cell debris, but also rare nuclear cell events. Since it is well known that most of the sorting protocols exclude events smaller than erythrocytes (less than 6 μ m in diameter) as debris or platelets, this fact may explain very well as to why unusually small VSELs were excluded in the past from the sorted cell populations.

Figure 1 (A and B) shows that in our proposed sorting strategy of VSELs, the size of the sorted cells is controlled very well by comparing them with the mixture of beads with predefined sizes (1, 2, 4, 6, 10 and 15 μm in diameter). The events enclosed in region R1, which include in average $47.2 \pm 2.1\%$ of total events, were further analysed for the expression of Sca-1 and lineage markers (Lin). The Sca-1⁺/Lin⁻ events shown in region R2 (Fig. 1D) consisted on average $0.38 \pm 0.05\%$ of total analysed BMMNCs. Since we employed in our 'lineage cocktail' the antibodies against Ter119, small cells from the erythroid lineage were excluded from our sorting populations. Cells from region R2 were subsequently sorted according to the expression of CD45 antigen and divided into Sca-1⁺/Lin⁻/CD45⁻ (region R3) and Sca-1⁺/Lin⁻/CD45⁺ (region R4) subpopulations (Fig. 1C) that contained VSELs and HSCs, respectively [1]. We found that VSELs comprised on average $0.030 \pm 0.008\%$ while HSCs $0.347 \pm 0.057\%$ of total BMMNCs (Fig. 1C).

Figure 1E shows the post-sort re-analysis of sorted VSELs, which revealed their high purity ($97.83 \pm 0.63\%$). At the same time, we demonstrated that $94.43 \pm 1.49\%$ of these cells were negative for staining with 7-AAD dye. We did not exclude anucleated debris from viable cells in this step (Fig. 1F). Thus, VSELs sorted from the murine BM via this novel strategy are homogeneous and viable population of cells (Fig. 1E and F).

In the next step, sorted VSELs were re-analysed according to their size. Figure 2A shows FSC/SSC characteristics of beads that were used as size markers for VSEL sorts. We noticed that $95.24 \pm 0.94\%$ of Sca-1⁺/Lin⁻/CD45⁻ (VSELs) were located within the 2–6 μm size range, while $85.82 \pm 1.28\%$ of Sca-1⁺/Lin⁻/CD45⁺ (HSCs) were in the 6–10 μm size range (Fig. 2B). Similar results were obtained when BMMNC population was analysed without the initial size restrictions (disregarding region R1), that is, only based on Sca-1, lineage markers and CD45 expression (Fig. 2C). Accordingly, our analysis revealed that $95.31 \pm 0.48\%$ of Sca-1⁺/Lin⁻/CD45⁻ VSELs were very small (2–6 μm in size) while $92.50 \pm 0.49\%$ of Sca-1⁺/Lin⁻/CD45⁺ HSCs were larger than 6 μm .

Thus, by employing flow cytometry and the size marker beads we have confirmed that the majority of Sca-1⁺/Lin⁻/CD45⁻ cells isolated from adult BM is unusually small (<6 μm). Thus, VSELs are larger than peripheral blood platelets and smaller than erythrocytes.

Confocal microscopic analysis confirms the unusually small size of purified VSELs

In our previous reports, the transmission electron microscopy (TEM) studies revealed that Sca-1⁺/Lin⁻/CD45⁻ VSELs are very small (2–4 μm in size) as compared with Sca-1⁺/Lin⁻/CD45⁺ HSCs, which are 8–10 μm in size [1–5]. TEM also revealed that VSELs possess relatively large nuclei containing open-type euchromatin, surrounded by a narrow rim of cytoplasm [1]. Confocal microscopic analysis of BM-derived HSCs and VSELs. Sorted Sca-1⁺/Lin⁻/CD45⁺ HSCs are relatively larger (>5 μm) and stain negative for Oct-4 (Fig. 3A). In contrast, VSELs are small (<5 μm) nucleated cells, do not express CD45 antigen on the surface, and express the embryonic stem cell transcription factor Oct-4 in the nucleus.

ImageStream analysis confirms the size of VSELs and efficiently distinguishes them from cell fragments

The IS-based analysis employs flow cytometry combined with microscopy and allows for (i) statistical analysis of a variety of cellular parameters as well as (ii) the visualization of cells in suspension during flow analysis via high-resolution brightfield, darkfield and fluorescence images [6–8]. The high resolution of IS imaging enables identification of objects as small as 1 μm in diameter [6–8].

Using IS, we evaluated the relative levels of Sca-1, Lineage markers and CD45 expression based on the fluorescence intensity. We also directly measured the diameter of individual cells based on brightfield imaging, and calculated the N/C ratio as well as the total cytoplasmic area from brightfield and fluorescence acquisitions. In order to assess the size of the cell nuclei and to prove that VSELs are not contaminated by large platelets, cell fragments, or enucleated cells from the erythroid lineage, total BM-derived cells were permeabilized and stained with DNA-binding dye (7-AAD). Importantly, the IS was configured to optimize fluorescence sensitivity without detector saturation that enabled collection of images of interest using cell classifiers that reduced the amount of debris and cell clumps in data files. A total of 3000 events were collected each time and analysed for the presence of VSELs (Fig. 4A).

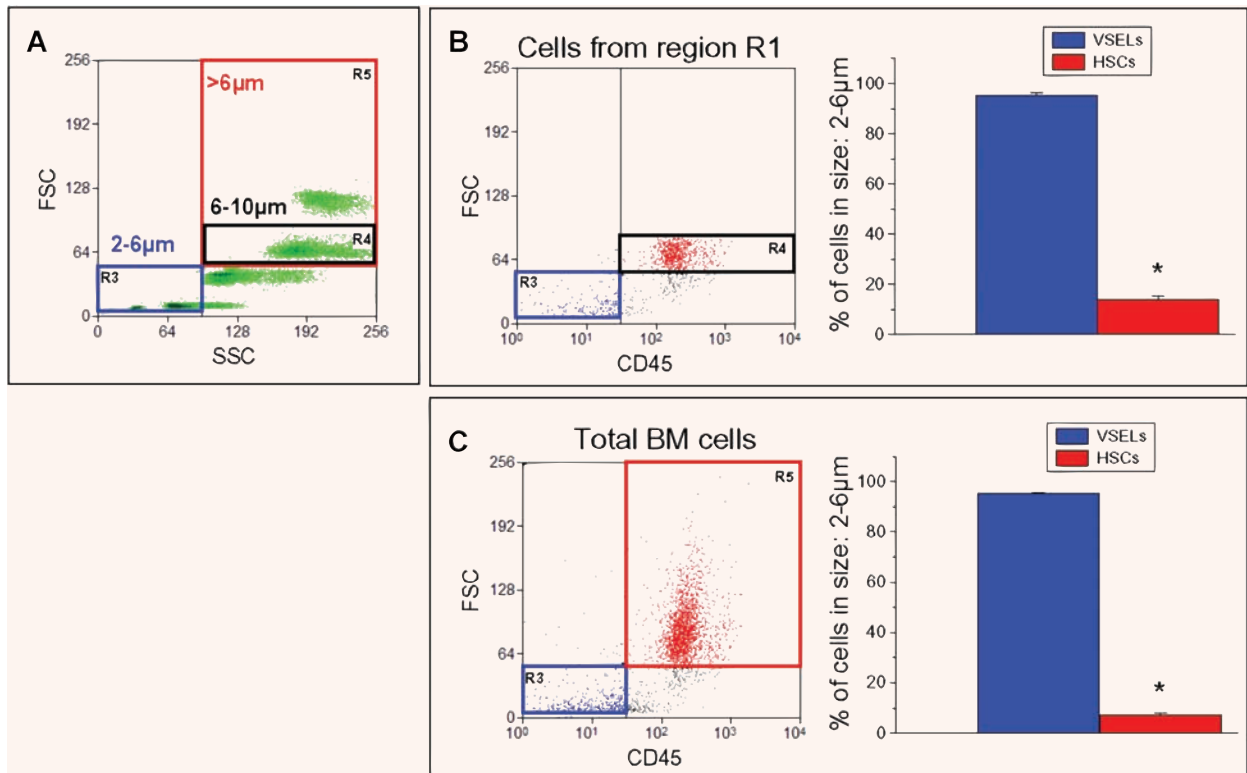


Fig. 2 Analysis of VSELs and HSCs according to the size. $Sca-1^{+}/Lin^{-}/CD45^{-}$ cells (VSELs) and $Sca-1^{+}/Lin^{-}/CD45^{+}$ cells (HSCs) were identified and analysed by FACS as shown previously. **B** and **C** shows the size analysis of $Sca-1^{+}/Lin^{-}/CD45^{-}$ cells (VSELs; blue) and $Sca-1^{+}/Lin^{-}/CD45^{+}$ cells (HSCs; red) in comparison to **(A)**. In accordance with bead size, the blue, black and red boxes on dot-plots contain events between 2 and 6 μm (region R3), 6–10 μm events (region R4), and >6 μm (region R5), respectively. **(B)** The size analysis of only small cells enclosed in region R1 (see Fig. 1B); right graph presents the percent of VSELs (blue bar) and HSCs (red bar) with the cell size between 2 and 6 μm . The majority of VSELs is enclosed in region R3 (blue box), while HSCs belong to region R4 (black box) containing events between 6 and 10 μm (left panel). **(C)** shows the size analysis of total BMMNC. Graph on the right presents the percentage of cells with VSELs' phenotype (blue bar) and HSCs' phenotype (red bar) with the size between 2 and 6 μm . The majority of HSCs belong to region R5 (red box) containing events larger than 6 μm (left panel). All values are presented as mean (SEM). *P*-values less than 0.05 are considered statistically significant (*).

Figure 4, panel B shows an image gallery of cells identified in total BM-derived population as VSELs by gating with regions R1, R2 and R3 (Fig. 4A) and confirmed their basic features including small size and expression of surface markers. By employing IS analysis we calculated with more precision that VSELs are very small ($3.63 \pm 0.14 \mu m$ in diameter), while $Sca-1^{+}/Lin^{-}/CD45^{+}$ HSCs are larger ($6.54 \pm 0.17 \mu m$ in diameter) (Fig. 5A). These observations are in agreement with our previous observations using electron microscopy [1], and the current findings using flow cytometry and confocal microscopy. Figure 5B shows an image gallery of examples of the sorted VSEL, HSC, polymorphonuclear

cell (PMNC) cell and Nalm-6 lymphoblast. As expected, VSELs are much smaller than HSCs and significantly smaller than peripheral blood granulocytes ($8.08 \pm 0.18 \mu m$ in diameter) or Nalm-6 cells.

Finally, we investigated the N/C ratio as well as the cytoplasmic area of VSELs (Figs 6 and 7) in comparison with HSCs, PMNCs and Nalm-6 cells. We noticed that VSELs have significantly higher ($P \leq 0.05$) N/C ratio as compared with HSCs, granulocytes and Nalm-6 cells (1.47 ± 0.17 , 0.82 ± 0.03 , 0.52 ± 0.02 and 0.70 ± 0.02 , respectively) (Fig. 7A). The cytoplasmic area was computed as the difference between the total cellular area, calculated based on the brightfield image, and the nuclear area. VSELs

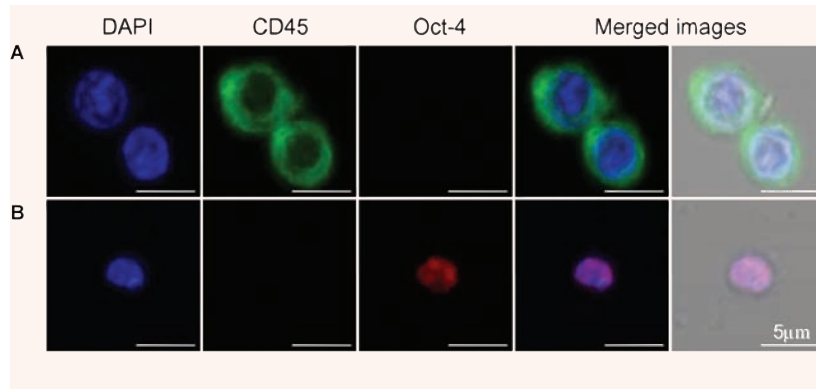


Fig. 3 Confocal microscopic images of VSELs and HSCs. Isolated VSELs and HSCs were stained for CD45 (FITC, green fluorescence) and Oct-4 (TRITC, red fluorescence). Nuclei were stained with DAPI (blue fluorescence). **(A)** shows Sca-1⁺/Lin⁻/CD45⁺ cells (HSCs) that are positive for CD45 and negative for Oct-4. **(B)** shows Sca-1⁺/Lin⁻/CD45⁻ cell (VSEL), negative for CD45 and positive for Oct-4, a marker of pluripotent cells.

had significantly ($P \leq 0.05$) lower cytoplasmic area as compared with HSCs, granulocytes, and Nalm-6 cells (5.41 ± 0.58 , 33.78 ± 1.68 , 52.33 ± 2.22 and $81.54 \pm 2.60 \mu\text{m}^2$, respectively) (Fig. 7B).

Discussion

Very small embryonic-like stem cells (VSELs) have been recently isolated and characterized from adult BM as well as other organs [1–3]. VSELs are the first adult tissue-derived primitive cell population with embryonic-like features that have been purified at the single cell level. Their major antigenic phenotype has been established as Sca-1⁺/Lin⁻/CD45⁻, however we reported that they also express CXCR4 receptor and CD133 antigen [1, 2, 9]. TEM analysis of VSELs revealed that they are small in size (2–4 μm range), contain relatively large nuclei surrounded by a narrow rim of cytoplasm, as well as open-type euchromatin in nuclei, which are characteristic features of pluripotent embryonic stem cells. More importantly, using RQ-PCR and immunohistochemistry, we have shown that murine VSELs express markers of embryonic pluripotent stem cells including SSEA-1, Oct-4, Nanog and Rex-1. Moreover, they are also enriched in mRNA for several early developmental markers and transcription factors for skeletal muscles, cardiac muscles, neural tissue, liver, intestinal epithelium, skin epidermis and endocrine pancreas [1, 2]. It is why we described initially these cells as tissue committed stem cells (TCSC) [9]. In cultures, VSELs are able to differentiate *in vitro* into neuronal cells, cardiomyocytes and pancreatic islet cells [1, 2]. When expanded over murine C2C12 myoblastic cell line, murine VSELs gave rise to spheres that resembled embryoid bodies [1, 5]. Further experiments

demonstrated that VSELs, normally residing in the BM, could be mobilized into peripheral blood in response to tissue/organ injury as well as after G-CSF treatment [2, 4, 10]. Recently, we have isolated a rare population of VSELs also from human cord blood (CB) [11], which suggests that these cells are also present in human tissues.

In the current study, we optimized the purification of VSELs, and perhaps more importantly, examined the morphological features of murine VSELs with greater precision and detail via the use of multiple imaging approaches. The traditional flow cytometric analysis of VSELs was complemented by confocal microscopy. Finally, the IS system, a new method that combines both flow cytometry and microscopic imaging, was used for quantitative analysis of cell size, N/C ratio and cytoplasmic area.

When examined by all methods employed in this study, murine VSELs are very small (<5 μm in diameter) when compared to Sca-1⁺/Lin⁻/CD45⁺ HSCs (>6 μm in size) and contain Oct-4⁺ relatively large nuclei surrounded by a narrow rim of cytoplasm. Therefore, since VSELs are smaller than erythrocytes, this fact may explain as to why in the past they were excluded from the routine sorting procedures. Our data clearly demonstrate the presence of small primitive nucleated cells in adult tissues that are slightly larger than blood platelets yet smaller than erythrocytes.

Generally, the presence of cells possessing similar small size (<5 μm) in adult murine tissues has been postulated recently by Vacanti *et al.* These cells were described as ‘spore-like stem cells’ [12]. Unfortunately the isolation strategy of spore-like stem cells was not described by the authors in the original paper and thus it is not clear as to how these cells were isolated from adult tissues. In contrast, by

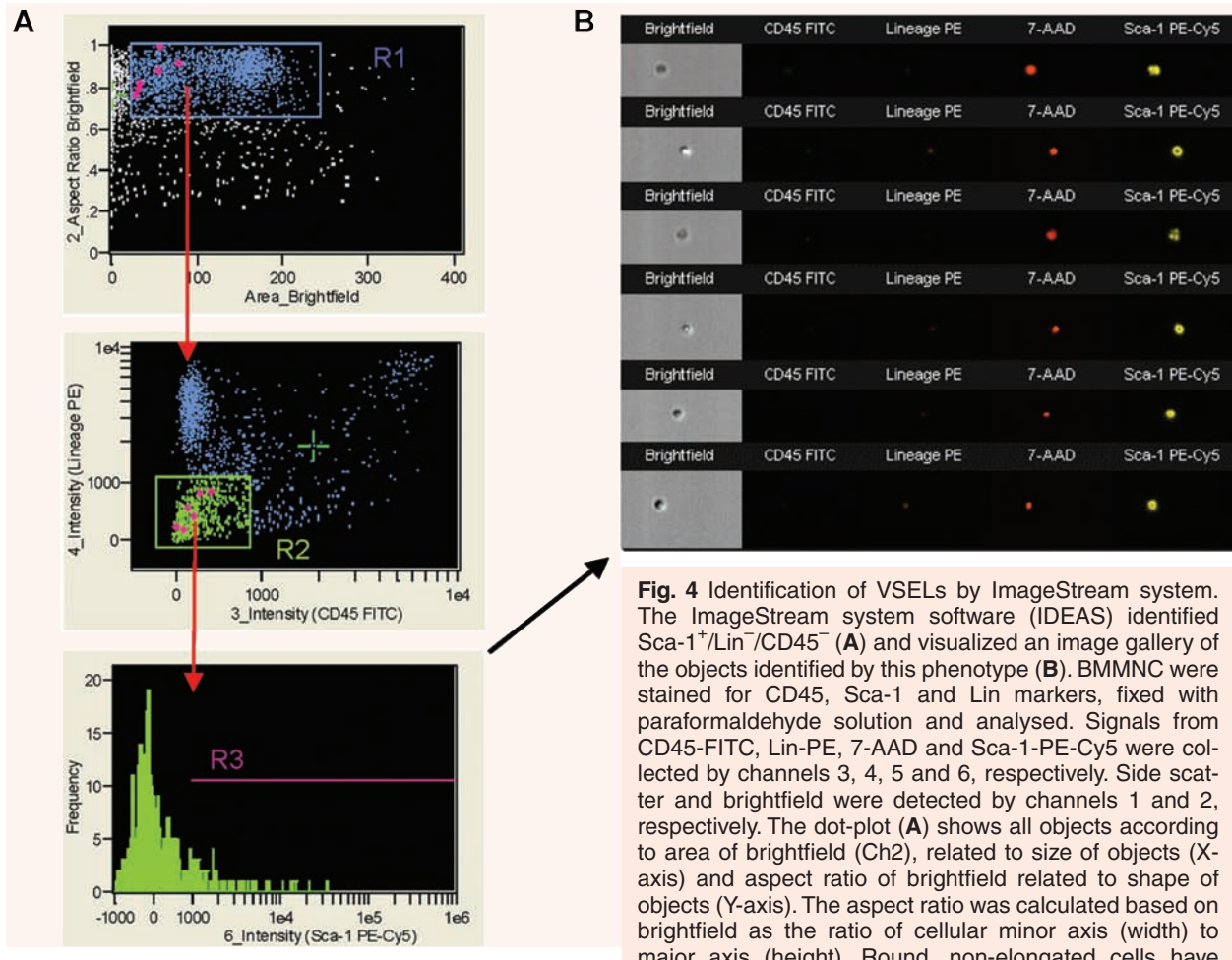


Fig. 4 Identification of VSELs by ImageStream system. The ImageStream system software (IDEAS) identified Sca-1⁺/Lin⁻/CD45⁻ (**A**) and visualized an image gallery of the objects identified by this phenotype (**B**). BMMNC were stained for CD45, Sca-1 and Lin markers, fixed with paraformaldehyde solution and analysed. Signals from CD45-FITC, Lin-PE, 7-AAD and Sca-1-PE-Cy5 were collected by channels 3, 4, 5 and 6, respectively. Side scatter and brightfield were detected by channels 1 and 2, respectively. The dot-plot (**A**) shows all objects according to area of brightfield (Ch2), related to size of objects (X-axis) and aspect ratio of brightfield related to shape of objects (Y-axis). The aspect ratio was calculated based on brightfield as the ratio of cellular minor axis (width) to major axis (height). Round, non-elongated cells have

aspect ratio close to 1.0, while the elongated cells or clumps had lower aspect ratio. When applied to bone marrow cells, region R1 encloses mostly single, round objects resembling cells. Subsequently, objects from region R1 are visualized according to their CD45 and Lin expression (X- and Y-axis, respectively; **A**, middle dot-plot). CD45⁻/Lin⁻ objects were included into region R2 and further analysed based on Sca-1 expression (**A**, lower histogram). (**B**) shows the image gallery of nucleated objects included into region R3 and defined as Sca-1⁺/Lin⁻/CD45⁻. Cells were fixed before staining with 7-AAD.

employing FACS-based phenotypic analysis of single cell suspensions prepared from murine brain, blood and intestinal epithelium, Howell *et al.* revealed the presence of very small CD45⁻Sca-1⁺c-kit⁻ cells in varying degrees that may represent universal pluripotent stem cells residing at different levels in multiple murine tissues [13]. Very small stem cells with neuroblast activity were also recently found in the murine brain in the subventricular zone [14]. Finally, Huang *et al.* described a population of very small cells residing in human BM while isolating mesenchymal stem cells (MSCs) on double layer culture plates contain-

ing 3-µm pores that were employed to sieve out the relatively large MSCs [15].

The size of VSELs and the expression of markers of pluripotency (Oct-4, Nanog, and Rex-1[1]) suggest that these cells could be directly derived from epiblasts and are deposited during development in various tissues (including BM) as a potential population of pluripotent stem cells that gives rise to tissue-specific stem cells [5, 11, 16, 17]. The potential relationship of our VSELs to Vacanti's spore-like stem cells, small cells identified in subventricular region of brain or cells isolated from BM by Huang *et al.* will require

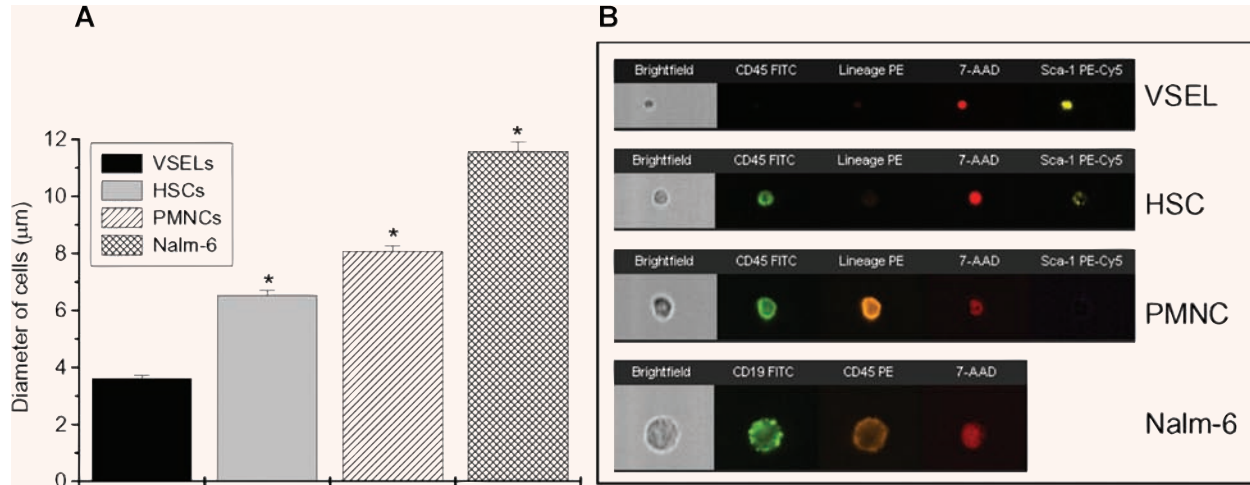


Fig. 5 Identification of size of VSELs and HSCs by ImageStream system. Cellular diameter analysis (**A**) and representative images (**B**) of murine and human cells illustrate their size and morphology. Panel A presents comparison of cellular diameter between murine BM-derived Sca-1⁺/Lin⁻/CD45⁻ (VSELs), Sca-1⁺/Lin⁻/CD45⁺ (HSCs), polymorphonuclear cells (PMNCs) isolated from blood and human leukaemia B cell (Nalm-6 cell line). Size of the cells was calculated based on the scale measurements employed by IDEAS software. Graph and table include mean ± S.E.M. *P* < 0.05 were considered statistically significant (*). (**B**) shows representative images of cells from each population. Panels show separate or merged images composed from brightfield, nuclear 7-AAD stained (red), CD45 (green), Lin (orange) and Sca-1 (yellow) by VSEL, HSC and PMNC. Expression of CD19 and CD45 by Nalm-6 cell is shown in green and orange, respectively.

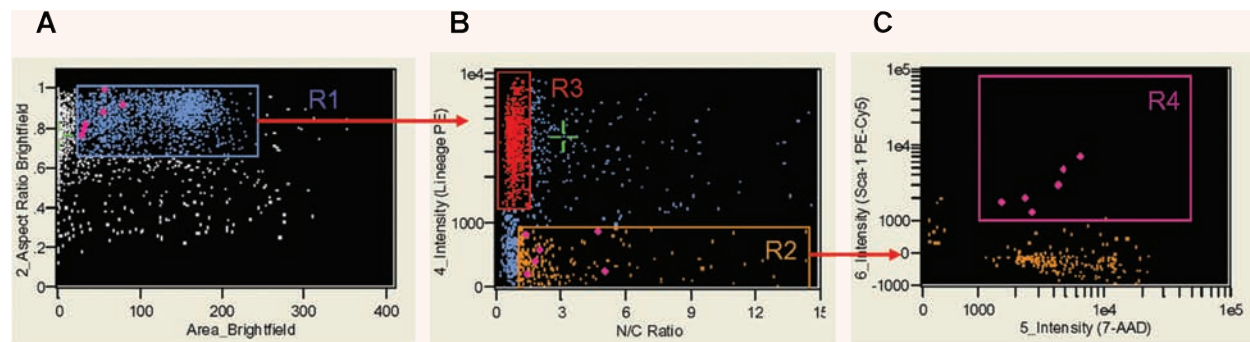
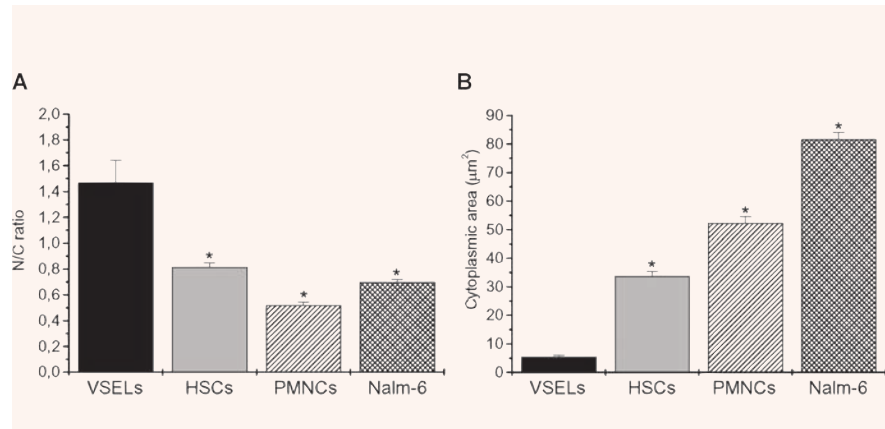


Fig. 6 Analysis of nuclear to cytoplasmic ratio by ImageStream system. Single, round cells from region R1 (**A**) were visualized based on their nuclear to cytoplasm ratio and Lin markers expression (X- and Y-axis, respectively (**B**)). Cellular populations were gated including Lin⁺ cells with low nuclear to cytoplasmic ratio (0.936 ± 0.016) (region R3, red) and Lin⁻ cells with high N/C ratio (3.485 ± 0.248) (region R2, orange). Objects from region R2 were further analysed for their CD45 and Sca-1 expression (X- and Y-axis, respectively (**B**)). Cells with VSELs' phenotype (Sca-1⁺/Lin⁻/CD45⁻) and characterized by higher N/C ratio ($1.471(0.171)$) were included in region R4 (magenta; **C**) and visualized on the other plots as diamonds (magenta). N/C ratio was calculated as nuclear area divided by cytoplasmic area computed from nuclear (7-AAD) and brightfield images. Signals of brightfield, Lin-PE and 7-AAD were collected by the IS in channels 2, 4 and 5, respectively. Mean (± S.E.M.) values of N/C ratio were calculated using IDEAS software.

further investigation. Of note, since our VSELs express CD133 on the surface [11], it is also likely that they are isolated along with larger cells in CD133⁺ population

of cells by employing immunomagnetic beads-based selection methods. In fact CD133⁺ cells isolated by magnetic beads were recently demonstrated to be

Fig. 7 N/C ratio and cytoplasmic area of VSELs. Mean N/C ratios (**A**) and cytoplasmic areas (**B**) of murine BM-derived Sca-1⁺/Lin⁻/CD45⁻ cells (VSELs) as well as Sca-1⁺/Lin⁻/CD45⁺ cells (HSCs), PB-derived granulocytes (PMNCs) and human Nalm-6 cells were measured using the IS. All values are presented as mean (\pm S.E.M. as calculated by IDEAS software. $P < 0.05$ was considered statistically significant (*).



enriched both for normal pluripotent [18] as well as cancer stem cells [19–21].

In the current paper we pursued characterizing the primitive markers, cell size and N/C ratio of VSELs in an attempt to further investigate their primitive nature and explore future strategies for their optimal isolation and better characterization. As a first step, we employed size beads with pre-defined diameters. Using direct comparison, the majority of VSELs were localized in the region occupied by 2–4 μm beads. Next, by employing staining with 7-AAD, a dye that is excluded by living cells, we were able to distinguish VSELs from potential dead cells. Using these approaches, we developed a sorting strategy directed towards isolating very small cells with greater accuracy. Although the relative cellular size can be estimated from forward scatter characteristics of cells (FSC) [22], an approximate estimation cannot be obtained without direct comparison with standard particles such as predefined beads [23, 24]. We employed ImageStream technology to accurately assess the size of VSELs.

Traditionally, confocal and electron microscopy have been used to evaluate cellular size and ultrastructure characteristics [25–31]. In the current study, we employed IS as an additional approach in evaluating both size and morphology of VSELs. The IS combines the capabilities of an advanced flow cytometer with the high-definition imaging of a fluorescent microscope. Historically, the first system to combine these two techniques was laser scanning cytometer (LSC) [32–37]. However, the IS provides the advantage of analyzing multiple cells in suspension which can not be achieved with LSC and allows for quantitative measurements of size, shape, tex-

ture, position of fluorochrome-labeled probes inside, on or between cells, as well as several nuclear features [6, 8, 38]. The IS technology provides high-resolution brightfield, darkfield and fluorescence images of cells; and analyses a wide array of cellular parameters in a relatively simple and time efficient manner. The high sensitivity and resolution (1 μm) of this system provides additional advantages when examining extremely small cells (*e.g.* VSELs).

We noticed that both cellular size and morphology determined by the IS were consistent with our previous results from confocal and electron microscopy. In agreement with microscopic results, the IS analysis confirmed the very small size of murine BM-derived VSELs, estimated at $<5\mu\text{m}$ ($3.63 \pm 0.09 \mu\text{m}$), while the size of Sca-1⁺/Lin⁻/CD45⁺ HSCs (controls) was $>6 \mu\text{m}$ ($6.54 \pm 0.17 \mu\text{m}$). Via DNA staining of sorted VSELs, IS allowed us to assess their purity and distinguish them easily from larger cell fragments, platelets, or small CD45⁻ differentiated cells from erythroid lineage.

Primitive stem cells have been described as small cells with large nucleus and small cytoplasmic area [27, 39, 40]. It has been proposed that with differentiation, cells acquire smaller nuclei as their cytoplasmic area enlarges. Thus, the IS analysis was used to calculate the nuclear and overall cellular areas as well as the N/C ratio of VSELs, HSCs, differentiated peripheral blood granulocytes and Nalm-6 cells. In agreement with the published data, the N/C ratio was significantly higher among primitive VSELs, followed by HSCs, than differentiated granulocytes and Nalm-6 cells. These observations support our hypothesis that VSELs are at an earlier stage of development compared with other multi-potent stem cells, such as HSCs. We also demonstrated that the cytoplasmic

area of VSELs is significantly smaller when compared with HSCs and differentiated blood cells. Although the cytoplasmic area is dependent on the cellular size, we believe that the smaller cytoplasmic area is indicative of the primitivity of VSELs especially when viewed in the context of high N/C ratio.

In conclusion, in the present study by employing a multi-dimensional approach, we confirmed the embryonic features of VSELs. In addition, we validated a novel size-based gating strategy to reliably isolate VSELs by FACS from murine BM. Using flow cytometry, confocal microscopy and ImageStream analysis we determined that VSELs are very small in size and have a relatively high N/C ratio when compared with other cell types. Therefore, FACS-based sorting strategies should consider that adult tissues harbour small primitive cells that are larger than platelets yet smaller than erythrocytes.

Acknowledgement

This work was supported by grants NIH DK074720 and NIH CA106281 to MZR, and by NIH AI057808 and DOD PC051290 to JWJL.

References

1. **Kucia M, Reza R, Campbell FR, Zuba-Surma E, Majka M, Ratajczak J, Ratajczak MZ.** A population of very small embryonic-like (VSEL) CXCR4(+)SSEA-1(+)Oct-4+ stem cells identified in adult bone marrow. *Leukemia*. 2006; 20: 857–69.
2. **Kucia M, Ratajczak J, Reza R, Janowska-Wieczorek A, Ratajczak MZ.** Tissue-specific muscle, neural and liver stem/progenitor cells reside in the bone marrow, respond to an SDF-1 gradient and are mobilized into peripheral blood during stress and tissue injury. *Blood Cells Mol Dis*. 2004; 32: 52–7.
3. **Kucia M, Ratajczak J, Ratajczak MZ.** Are bone marrow stem cells plastic or heterogenous-that is the question. *Exp Hematol*. 2005; 33: 613–23.
4. **Kucia M, Ratajczak MZ.** Stem cells as a two edged sword - from regeneration to tumor formation. *J Physiol Pharmacol*. 2006; 57: 5–16.
5. **Kucia M, Zuba-Surma E, Wysoczynski M, Dobrowolska H, Reza R, Ratajczak J, Ratajczak MZ.** Physiological and pathological consequences of identification of very small embryonic like (VSEL) stem cells in adult bone marrow. *J Physiol Pharmacol*. 2006; 57: 5–18.
6. **George TC, Basiji DA, Lynch DH, Ortyn WE, Perry DJ, Seo MJ, Zimmerman CA, Morrissey PJ.** Distinguishing modes of cell death using the ImageStream multispectral imaging flow cytometer. *Cytometry A*. 2004; 59A: 237–45.
7. **Ortyn WE, Hall BE, George TC, Frost K, Basiji DA, Perry DJ, Zimmerman CA, Coder DC, Morrissey PJ.** Sensitivity Measurement and Compensation in Spectral Imaging. *Cytometry A*. 2006; 69A: 852–62.
8. **George TC, Fanning SL, Fitzgeral-Bocarsly P, Medeiros RB, Highfill S, Shimizu Y, Hall BE, Frost K, Basiji D, Ortyn WE, Morrissey PJ, Lynch DH.** Quantitative measurement of nuclear translocation events using similarity analysis of multispectral cellular images obtained in flow. *J Immunol Methods*. 2006; 311: 117–29.
9. **Kucia M, Ratajczak J, Ratajczak MZ.** Bone marrow as a source of circulating CXCR4+ tissue-committed stem cells. *Biol Cell*. 2005; 97: 133–46.
10. **Kucia M, Dawn B, Hunt G, Guo Y, Wysoczynski M, Majka M, Ratajczak J, Rezzoug F, Ildstad ST, Bolli R, Ratajczak MZ.** Cells expressing early cardiac markers reside in the bone marrow and are mobilized into the peripheral blood after myocardial infarction. *Circ Res*. 2004; 95: 1191–9.
11. **Kucia M, Halasa M, Wysoczynski M, Baskiewicz-Masiuk M, Moldenhawer S, Zuba-Surma E, Czajka R, Wojakowski W, Machalinski B, Ratajczak MZ.** Morphological and molecular characterization of novel population of CXCR4(+) SSEA-4(+) Oct-4(+) very small embryonic-like cells purified from human cord blood - preliminary report. *Leukemia*. 2007; 21: 297–303.
12. **Vacanti MP, Roy A, Cortiella J, Bonassar L, Vacanti CA.** Identification and initial characterization of spore-like cells in adult mammals. *J Cell Biochem*. 2001; 80: 455–60.
13. **Howell JC, Lee WH, Morrison P, Zhong J, Yoder MC, Srour EF.** Pluripotent stem cells identified in multiple murine tissues. *Ann NY Acad Sci*. 2003; 996: 158–73.
14. **Scheffler B, Walton NM, Lin DD, Goetz AK, Enikolopov G, Roper SN, Steindler DA.** Phenotypic and functional characterization of adult brain neurogenesis. *Proc Natl Acad Sci USA*. 2005; 102: 9353–8.
15. **Hung SC, Chen NJ, Hsieh SL, Li H, Ma HL, Lo WH.** Isolation and characterization of size-sieved stem cells from human bone marrow. *Stem Cells*. 2002; 20: 249–58.
16. **Ratajczak MZ, Machalinski B, Wojakowski W, Ratajczak J, Kucia M.** A hypothesis for an embryonic origin of pluripotent Oct-4(+) stem cells in adult bone marrow and other tissues. *Leukemia*. 2007; 21: 860–7.

17. **Kucia M, Wu W, Ratajczak MZ.** Bone marrow-derived very small embryonic-like stem cells: Their developmental origin and biological significance. *Dev Dyn.* 2007; 236: 330–20.
18. **Baal N, Reisinger K, Jahr H, Bohle RM, Liang O, Münstedt K, Rao CV, Preissner KT, Zygmunt MT.** Expression of transcription factor Oct-4 and other embryonic genes in CD133 positive cells from human umbilical cord blood. *Thromb Haemost.* 2004; 92: 767–75.
19. **O'Brien CA, Pollett A, Gallinger S, Dick JE.** A human colon cancer cell capable of initiating tumour growth in immunodeficient mice. *Nature.* 2007; 445: 106–10.
20. **Ricci-Vitiani L, Lombardi DG, Pilozzi E, Biffoni M, Todaro M, Peschle C, De Maria R.** Identification and expansion of human colon-cancer-initiating cells. *Nature.* 2007; 445: 111–5.
21. **Singh SK, Clarke I, Terasaki M, Bonn VE, Hawkins C, Squire J, Dirks PB.** Identification of a cancer stem cell in human brain tumors. *Cancer Res.* 2003; 63: 5821–8.
22. **Shapiro HM.** Parameters and Probes. In: Practical Flow Cytometry. 4th ed. *John Wiley & Sons, Inc.*; 2005. pp. 275–6.
23. **Tocchetti EV, Flower RL, Lloyd JV.** Assessment of *in vitro*-generated platelet microparticles using a modified flow cytometric strategy. *Thromb Res.* 2001; 103: 47–55.
24. **De Paiva CS, Pflugfelder SC, Li DQ.** Cell size correlates with phenotype and proliferative capacity in human corneal epithelial cells. *Stem Cells.* 2006; 24: 368–75.
25. **Kouri JB, Arguello C, Luna J, Mena R.** Use of microscopical techniques in the study of human chondrocytes from osteoarthritic cartilage: an overview. *Microsc Res Tech.* 1998; 40: 22–36.
26. **Latimer P.** Light scattering vs. microscopy for measuring average cell size and shape. *Biophys J.* 1979; 27: 117–26.
27. **Romano AC, Espana EM, Yoo SH, Budak MT, Wolosin JM, Tseng SC.** Different cell sizes in human limbal and central corneal basal epithelia measured by confocal microscopy and flow cytometry. *Invest Ophthalmol Vis Sci.* 2003; 44: 5125–9.
28. **Teodori L, Albertini MC, Uguccione F, Falcier E, Rocchi MB, Battistelli M, Coluzza C, Piantanida G, Bergamaschi A, Magrini A, Mucciato R, Accorsi A.** Static magnetic fields affect cell size, shape, orientation, and membrane surface of human glioblastoma cells, as demonstrated by electron, optic, and atomic force microscopy. *Cytometry A.* 2006; 69: 75–85.
29. **Xiao JC, Jin XL, Ruck P, Adam A, Kaiserling E.** Hepatic progenitor cells in human liver cirrhosis: immunohistochemical, electron microscopic and immunofluorescence confocal microscopic findings. *World J Gastroenterol.* 2004; 10: 1208–11.
30. **He ZP, Tan WQ, Tang YF, Zhang HJ, Feng MF.** Activation, isolation, identification and *in vitro* proliferation of oval cells from adult rat livers. *Cell Prolif.* 2004; 37: 177–87.
31. **Petropavlovskaja M, Rosenberg L.** Identification and characterization of small cells in the adult pancreas: potential progenitor cells? *Cell Tissue Res.* 2002; 310: 51–8.
32. **Bedner E, Li X, Gorczyca W, Melamed MR, Darzynkiewicz Z.** Analysis of apoptosis by laser scanning cytometry. *Cytometry.* 1999; 35: 181–95.
33. **Darzynkiewicz Z, Bedner E, Li X, Gorczyca W, Melamed MR.** Laser-Scanning Cytometry: A New Instrumentation with Many Applications. *Exp Cell Res.* 1999; 249: 1–12.
34. **Darzynkiewicz Z, Huang X, Okafuji M.** Detection of DNA strand breaks by flow and laser scanning cytometry in studies of apoptosis and cell proliferation (DNA replication). *Methods Mol Biol.* 2006; 314: 81–93.
35. **Deptala A, Bedner E, Darzynkiewicz Z.** Unique analytical capabilities of laser scanning cytometry (LSC) that complement flow cytometry. *Folia Histochem Cytobiol.* 2001; 39: 87–9.
36. **Kamentsky LA.** Laser scanning cytometry. *Methods Cell Biol.* 2001; 63: 51–87.
37. **Kamentsky LA, Burger DE, Gershman RJ, Kamentsky LD, Luther E.** Slide-based laser scanning cytometry. *Acta Cytol.* 1997; 41: 123–43.
38. **Glisic-Milosavljevic S, Waukau J, Jana S, Jailwala P, Rovensky J, Ghosh S.** Comparison of apoptosis and mortality measurements in peripheral blood mononuclear cells (PBMCs) using multiple methods. *Cell Prolif.* 2005; 38: 301–11.
39. **Chen W, Hara K, Tian Q, Zhao K, Yoshitomi T.** Existence of small slow-cycling Langerhans cells in the limbal basal epithelium that express ABCG2. *Exp Eye Res.* 2007; 84: 626–34.
40. **Redvers RP, Li A, Kaur P.** Side population in adult murine epidermis exhibits phenotypic and functional characteristics of keratinocyte stem cells. *Proc Natl Acad Sci USA.* 2006; 103: 13168–73.